REPORT DOCUMENTATION PAGE		Form Approved OMB No. 0704-0188

Public reporting burden for this collection of information is estimated to average 1 hour per response, including the time for reviewing instructions, searching existing data sources, gathering and maintaining the data needed, and completing and reviewing the collection of information. Send comments regarding this burden estimate or any other aspect of this collection of information, including suggestions for reducing this burden, to Washington Headquarters Services, Directorate for Information Operations and Reports, 1215 Jefferson Davis Highway, Suite 1204, Arlington, VA 22202-4302, and to the Office of Management and Budget, Paperwork Reduction Project (0704-0188), Washington, DC 20503.

1. AGENCY USE ONLY (Leave blank)	2. REPORT DATE 24.May.05	3. REPORT TYPE AND DATES COVERED MAJOR REPORT

4. TITLE AND SUBTITLE
OPEN HOLE MULTILAYER FATIGUE CRACK GROWTH IN GLARE UNDER
COMBINED TENSION BENDING

5. FUNDING NUMBERS

6. AUTHOR(S)
MAJ RANDELL CHRISTIAN E

7. PERFORMING ORGANIZATION NAME(S) AND ADDRESS(ES)
DELFT UNIVERSITY

8. PERFORMING ORGANIZATION REPORT NUMBER

CI04-1092

9. SPONSORING/MONITORING AGENCY NAME(S) AND ADDRESS(ES)
THE DEPARTMENT OF THE AIR FORCE
AFIT/CIA, BLDG 125
2950 P STREET
WPAFB OH 45433

10. SPONSORING/MONITORING AGENCY REPORT NUMBER

11. SUPPLEMENTARY NOTES

12a. DISTRIBUTION AVAILABILITY STATEMENT
Unlimited distribution
In Accordance With AFI 35-205/AFIT Sup 1

12b. DISTRIBUTION CODE

13. ABSTRACT (Maximum 200 words)

DISTRIBUTION STATEMENT A
Approved for Public Release
Distribution Unlimited

14. SUBJECT TERMS	15. NUMBER OF PAGES 12
	16. PRICE CODE

17. SECURITY CLASSIFICATION OF REPORT	18. SECURITY CLASSIFICATION OF THIS PAGE	19. SECURITY CLASSIFICATION OF ABSTRACT	20. LIMITATION OF ABSTRACT

Standard Form 298 (Rev. 2-89) (EG)
Prescribed by ANSI Std. 239.18
Designed using Perform Pro, WHS/DIOR, Oct 94

OPEN HOLE MULTILAYER FATIGUE CRACK GROWTH IN GLARE UNDER COMBINED TENSION BENDING

Christian E. Randell, Jaap Schijve, Sybrand van der Zwaag

Faculty of Aerospace Engineering
Technical University of Delft, Delft, The Netherlands

Key Words: Fatigue, Fibre Metal Laminates, Glare, Open Hole, Subsurface Cracks

Abstract. This paper involves the development of an analytical/numerical crack growth model to predict surface and subsurface fatigue crack growth in the fibre metal laminate (FML) Glare subjected to combined tension and bending. The stress intensity factor for Glare can be divided into two parts: the stress intensity due to the crack opening stresses, and the stress intensity due to the fibre bridging stresses. The first component is derived from a stress intensity formulation for specimen geometry of monolithic aluminum. The second component is dependent upon the shape of the delamination surrounding the crack and the stresses in the fibres. Delamination shapes were taken from experimental observations, and fibre-bridging stresses were extracted from FEM. Using this approach, predictions are made on crack growth in the Glare surface layer and sub-surface layers. A new milled open-hole tension bending (MOHTB) fatigue specimen was developed to induce combined tension and bending in Glare specimens. This configuration avoids plastic deformations and spurious fatigue cracking observed in standard open-hole tension bending specimens. Fatigue tests were carried out on Glare 2A-5/4-0.4 and Glare 2A-6/5-0.4 specimens at σ_{app} = 80MPa and 100MPa with a stress ratio of 0.1. Data on the crack initiation periods in each of the layers are also presented. The comparison between the predicted fatigue crack growth in the aluminum layers and the experimental observations indicated a good agreement both for shape and scale of the crack growth curves.

1. Introduction

Glare is a member of the family of material systems known as Fibre Metal Laminates (FMLs). FMLs are characterized by their construction of alternating layers of metal and uniaxial fibers. Glare in particular consists of thin (between 0.3mm and 0.5mm typically) aluminum sheets and uniaxial glass fibres. The glass fibres are laid up in various configurations of ply orientation to maximize material properties for a given application e.g. as a skin material for aerospace applications. Slow fatigue crack growth rates in Glare make it an ideal candidate for aircraft applications – especially at the joint areas, where cracks typically initiate at the interface between the joined sheets and secondary bending is significant.

Fatigue crack growth characteristics for surface and through thickness cracks in Glare are relatively well understood[1-4]. However, further knowledge is needed about how cracks propagate at the subsurface level in a combined tension and bending environment. This environment allows cracks to initiate and propagate at different times and rates, as the different plies of Glare are subjected to differing levels of stress.

Past studies into fatigue cracks under combined tension and bending utilized variants of the open-hole tension-bending (OHTB) specimen[2,5,6]. In these specimens, a test section is fastened to two sheets by adhesive bonding. The eccentricity in the neutral line results in significant secondary bending in the test section, and thus a combined tension bending stress state is achieved when the specimen is placed in tension. By changing the overlap

dimensions, the ratio of tension to bending stress, i.e. the bending factor, k_b, can be varied. The value of k_b can be predicted through the use of the Neutral Line Model developed by Schijve[7]. The open hole acts as a blunt notch to encourage crack initiation, and mimics the rivet hole in an aircraft joint.

This paper tries to answer the question of whether subsurface crack growth in Glare under combined tension and bending is predictable. The first section discusses the development of an analytical model that makes use of finite element modeling (FEM) to acquire data that is not accessible experimentally. The second section discusses the experiments carried out to acquire crack growth data. In the Results and Discussion section, the model predictions are compared to experimental data to assess its legitimacy. Finally, conclusions are drawn from the results and analysis.

2. Analytical/Numerical Modeling

Unlike in monolithic materials, two types of stresses govern the local stresses around a crack tip in Glare. The first is the macroscopic stress resulting from the applied load. The applied load and specimen geometry govern the resulting stress intensity. The second stress, typical for FMLs, is the stress in the fibres in a zone around the crack: the fibre-bridging stress. These two stress types are superimposed to develop a total stress intensity factor for the specimen. In view of the assumed elastic behavior, the superposition is justified.

Tada[8] gives the Mode I stress intensity factor for a crack emanating from an open hole in a specimen undergoing pure tension as:

$$K_{I(OH)} = \sigma \sqrt{\pi a} \left\{ 0.5(3-s) \left[1 + 1.243(1-s)^3 \right] \right\}$$ (1)

where

$$s = \frac{a}{a+R}$$ (2)

where a is the crack length and R is the open hole radius. This formulation is applicable to the present tension-bending configuration as the bending load merely changes the tension stress in the individual plies of the specimen. The stress states within the individual plies of the specimen are in varying levels of tension. The average value of the stress state through the thickness of the individual plies is used in Eq.1.

The second, and more complicated stress intensity formulation is generated from the effects of the fibre bridging. An important feature of the stress intensity factor formulation for fibre bridging is that the fibre bridging stresses act at the delamination front – not on the crack face. Similarly, the fibre bridging stress distribution is not uniform – the fibres bridging the crack do not all carry the same load. To incorporate these two non-uniform aspects that comprise the fibre bridging, the stress intensity factor for a symmetric set of point loads arrayed around a crack is used. Tada[8] gives the basic formulation for the Mode I stress intensity factor for an array of point loads around a crack. Marissen[3] rewrote the expression in a form with only real variables:

$$K = P \sqrt{\frac{2a}{\pi}} \left\{ \frac{B}{A} + y_o^2 (1+v) \left(\frac{BC}{A^{3/2}} - \frac{\sqrt{A}+C}{2AB} \right) \right\}$$ (3)

where:

$$A = \left(a^2 - x_o^2 + y_o^2\right)^2 + 4x_o^2 y_o^2 \qquad (4)$$

$$B = \sqrt{a^2 - x_o^2 + y_o^2 + \sqrt{A}} \qquad (5)$$

$$C = a^2 + x_o^2 + y_o^2 \qquad (6)$$

where x_o and y_o locate the point of application of the stress -- here the fibre bridging stress applied at the delamination front. The term P is the applied load and v is the Poisson's ratio of the aluminum plies. While Eq. 6 applies to a sheet without a hole, its use is justified here as the effect of the open hole may be expected to be small for longer cracks.

To acquire the variable y_o in the above expression, the delamination shapes were measured. The delamination shapes change as the cracks extend. To describe the delamination front, b(x), in analytical terms, two different shape functions are used. For cracks less than 5mm in length, the shape is assumed to be triangular. For cracks greater than 5mm, a cosine function is applied.

$$b(x) = (-0.2)x + (0.2)(a+R) \qquad \text{a <5 mm, x=0-5 mm} \qquad (7)$$

$$b(x) = 0.2x\cos\left(\frac{x-R}{a-R}\right)\left(\frac{\pi}{2}\right) \qquad \text{a >5 mm, x=5-20 mm} \qquad (8)$$

As shown by Alderliesten[9], the actual delamination shape falls between both assumed shapes.

The non-uniform fibre bridging stress distribution was determined through finite element modeling (FEM). A model was constructed using the Abaqus finite element package that represented the MOHTB specimen as shown in Figure 1. One quarter of the specimen was modeled, with symmetry constraints applied along the length (x-direction) and width (y-direction) of the model. The plies were modeled individually, and were positioned on top of each other to build the laminate.
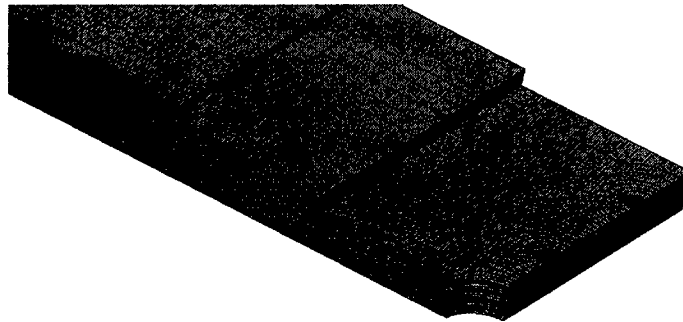

Figure 1: Typical FEM mesh of MOHTB specimen G2A-5/4-0.4.

Plies were bound together using tie constraints, which cause coincident nodes to move together as one node. Cracks were modeled by removing the symmetry constraints in the

loading-direction on the crack face of each cracked ply. This allowed the cracks to open when loads were applied, as there were no longer any constraints restricting displacements in the loading direction.

The first step to modeling the delaminations was to place seed nodes along the delamination front between plies. Elements were then formed around these seed nodes so the delamination front became the boundary between elements. In order to ensure that each surface had the same mesh applied, these seed nodes were imposed on each surface of each ply of the model. This allowed the tie constraints between plies in undelaminated regions to be preserved. This meshing created the regions to introduce delaminations. These regions were the interface between cracked aluminum plies and their adjacent prepreg plies behind the delamination fronts. The tie constraints were removed in the delaminated regions. This allowed the glass fibres to bridge the cracks. For subsurface cracks, the delamination regions above and below the crack are assumed to be identical.

Due to the bending load induced, the fibres on one side of a cracked aluminum ply carry a different load than the fibres on the other side of the ply. The fibre bridging stress applied to a cracked aluminum ply in the analytical model was taken as the average of the stresses found above and below the ply in the FEM. To find these fibre bridging stresses around a crack in an individual ply of the laminate, two model runs were required. Both runs utilized the same mesh in order to extract data from the same locations along the delamination fronts.

The first run included cracks and delaminations in plies from the surface down to, but not including, the ply of interest. This run provided strains in the fibres due to the damage in the plies closer to the surface than the one of interest as well as the strains due to the loading of the specimen, $\varepsilon_f(x)$. The second run added the crack and delaminations in the ply of interest. The strains from this run were similarly recorded, $\varepsilon_{fd}(x)$. The results of the first run were subtracted from the results of the second run to arrive at the strains in the glass fibres attributed to fibre bridging of the crack in the aluminum ply, $\varepsilon_{fb}(x)$.

$$\varepsilon_{fb}(x) = \varepsilon_{fd}(x) - \varepsilon_f(x) \tag{9}$$

Given the nature of the glass fibres, the fibre bridging stress distribution resulting from the fibre bridging strains were determined through simple material properties:

$$\sigma_{fb}(x) = E_f \varepsilon_{fb}(x) \tag{10}$$

Figure 2a shows a typical fibre bridging stress distribution for surface cracks in the specimens investigated. FEM runs for each specimen configuration were conducted for multiple crack lengths. The FEM results show a distribution that is comprised of two parts. The first part comprises stresses in the fibers that bridge over the flanks of the crack. This stress remains essentially the same along the flanks for any given crack length. The stress level does drop as the cracks lengthen. The second part comprises the stress spike at the crack tip. This rise is expected as the fibres have not delaminated significantly in this region and any COD in the metal plies imparts a large strain in the adjacent fibres.

These fibre bridging stress distributions were incorporated into the analytical model by applying a simplified representation, shown in Figure 2b. This representation breaks the fibre bridging distribution into two components, σ_{flank} and σ_{tip}. The first component, σ_{flank}, accounts for the stresses along the delamination front from the open hole to near the crack tip. The second component, σ_{tip}, captures the stress spike at the crack tip.
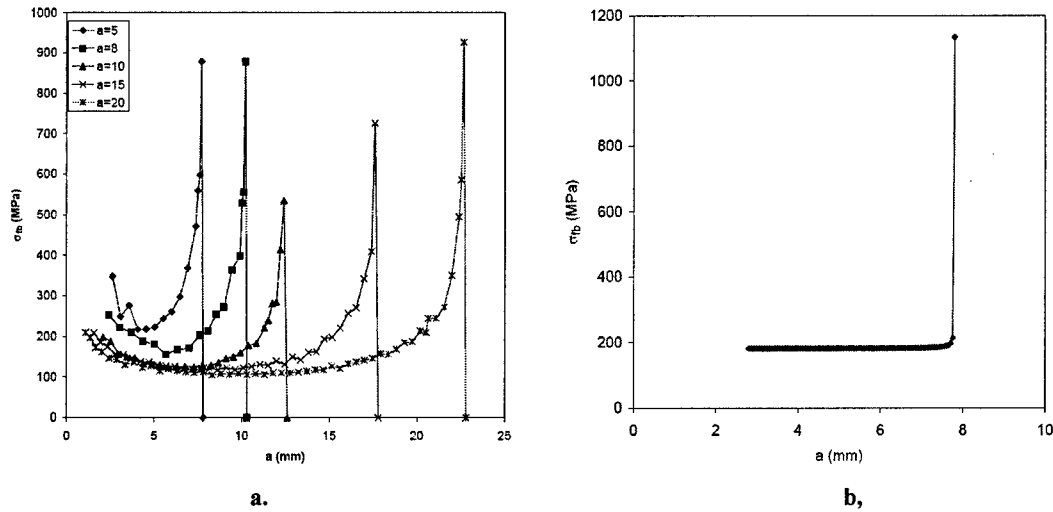
Figure 2: a: Typical fibre bridging stress distribution. Glare 2A-5/4-0.4. σ_{app} = 100 MPa.
b: Notional fibre bridging stress distribution representation used in analytical model.

The drop in σ_{flank} as the cracks grow has a direct effect on the crack growth prediction. A trend was noticed in the FEM results of σ_{flank} values versus modeled crack length. For a given specimen, the σ_{flank} values always fell on the same shaped curve – regardless of the ply investigated. For different specimens, the same shape of curve was observed; only the stress levels were shifted. A curve fit was applied to match this distribution, as shown in Equation 11. To apply this distribution shape to a given specimen, the distribution was offset as a function of the resulting stress found in the surface aluminum ply with the applied load in place, but prior to introduction of fatigue cracks.

$$\sigma_{flank} = (0.6\sigma_{res} + 220) - 185e^{-60*a^{-3.5}}$$ (11)

The fibre bridging stress at the tip of the crack, σ_{tip}, is difficult to assess, as it is very dependant upon the FEM mesh. As the results of the FEM show values well above the failure limit of the fibres, a constant value of 90% of the failure stress of the fibres was utilized. This is deemed appropriate as the FEM results do show a spike in stress at the crack tip, but experimental results do not show fibre breakage. The value of σ_{tip} must be less than the failure limit. The tip stress is applied over the final 0.5mm of the crack to ensure inclusion of the plastic zone at the tip of the crack. Sensitivity studies of the effects of σ_{tip} on the predicted crack growth rates show that the term plays a minor role in comparison to the flank stress.

The resulting expression for the fibre bridging stress applied to the analytical model took the form:

$$\sigma_{fb}(x) = \begin{cases} \sigma_{flank} & \text{for } 0 < x < (a - 0.5) \\ \sigma_{tip} & \text{for } (a - 0.5) < x < a \end{cases}$$ (12)

Using the fibre bridging stress distribution and delamination shape thus defined, the stress intensity factor was determined. Marissen[3] integrated the stress intensity, $K_{I(fb)}$, expression

over an elliptical delamination shape with a constant fibre bridging load. This allowed him to arrive at a relation between the stress intensity factor due to fibre bridging and a constant fibre-bridging load applied to a center cracked tension specimen. Incorporating the non-uniform stress distribution and the appropriate approximation of the delamination shape to his expansion yields:

$$K_{I(fb)} = \sqrt{\frac{2a}{\pi}} \int_{R}^{a} \sigma_{fb}(x) \left\{ \frac{B}{A} + y_o^2(1+v)\left(\frac{BC}{A^{3/2}} - \frac{\sqrt{A}+C}{2AB} \right) \right\} dx \tag{13}$$

with

$$x_o = x \tag{14}$$

$$y_o = b(x) \tag{15}$$

The terms A, B and C are identical to those defined in Equations 4-6. The limits on the above integration range from x = R (the edge of the open hole, where the crack length is zero), to the final crack length, x = a.

Using both contributing Mode I stress intensity factor formulations found in Equations 1 and 13, the principal of superposition is used to arrive at a total stress intensity factor for the fatigue crack in the MOHTB specimen.

$$K_{I(tot)} = K_{I(OH)} - K_{I(fb)} \tag{16}$$

$$K_{I(tot)} = \sigma\sqrt{\pi a}\left\{0.5(3-s)\left[1+1.243(1-s)^3\right]\right\} -$$
$$\sqrt{\frac{2a}{\pi}} \int_{R}^{a} \sigma_{fb}(x) \left\{ \frac{B}{A} + y_o^2(1+v)\left(\frac{BC}{A^{3/2}} - \frac{\sqrt{A}+C}{2AB} \right) \right\} dx \tag{17}$$

From this a stress intensity factor range can be developed to allow for crack growth predictions using simple Paris law formulations.

$$\frac{da}{dN} = C\left(\Delta K_{I(tot)}\right)^n \tag{18}$$

where C and n are the material constants for the metal constituents. For the aluminum alloys used in this study, C and n values are taken from literature[10] on through crack modeling and are 2.7E+12 and 2.94, respectively. Comparisons of predicted crack growth and experimental results are given below.

3. Experimentation

Experiments were conducted to evaluate the fatigue characteristics of Glare specimens under a combined tension and bending load state. Of interest was the growth rates of fatigue cracks in subsurface layers of the laminates. The variant of the OHTB specimen in Fig. 4 was initially adopted to study fatigue crack growth in Glare under combined tension and bending. This classical specimen setup has the advantages of being easy to manufacture, and simple to

design to achieve the desired stress state[11]. This specimen, however, exhibited unwanted plastic deformation at the areas of the overlaps, leading to an uncontrolled release of the bending moment during the course of the experiment. Additionally, fatigue cracks formed around the fastener holes during testing. These occurrences made it impossible to predict the stress state in the test section with the open hole.
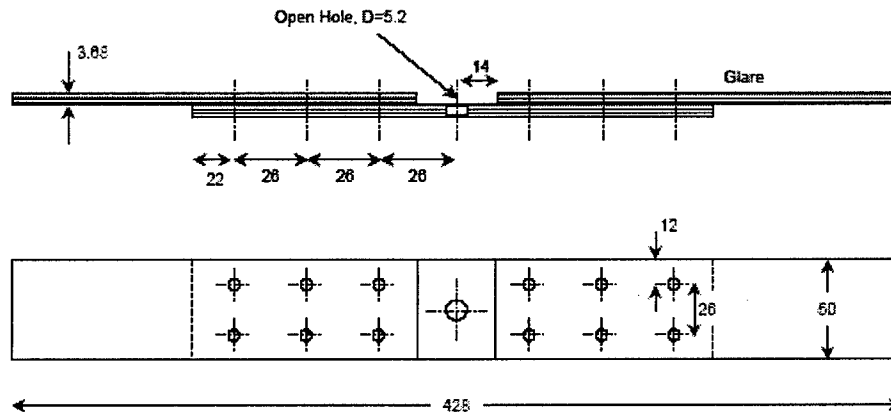

Figure 4: Open Hole Tension Bending (OHTB) specimen configuration for Glare.

To overcome these difficulties, a new specimen geometry and manufacturing method was designed, leading to a novel test geometry: the Milled Open Hole Tension Bending (MOHTB) specimen[12]. The MOHTB specimen in Figure 5 was machined from a relatively thick plate of Glare by tapering the thickness to obtain secondary bending under tension loads. The gradual shift in the eccentricity of the neutral line effectively reduces stress concentrations present in the overlaps of the OHTB specimen, and insures no loss of bending moment due to settling of the overlaps.

No plastic deformation in the test section was noted in the specimen following testing. Furthermore, machining the specimen from a single thick plate eliminates the need for fasteners to attach the sheets used in the OHTB specimen. This removed the chance of fatigue cracks forming away from the test section of the specimen around fastener holes.
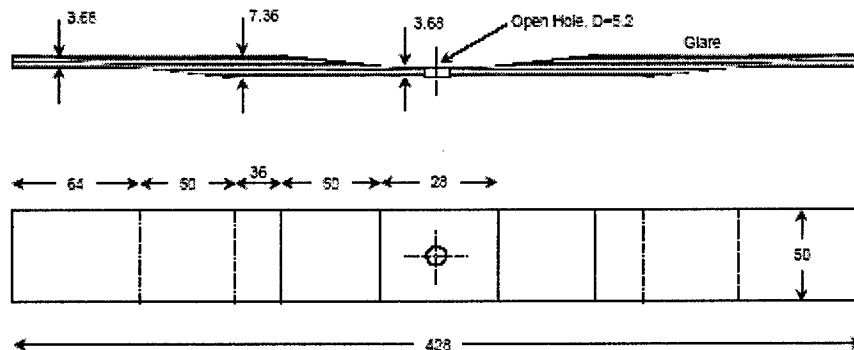

Figure 5: Milled Open Hole Tension Bending (MOHTB) specimen configuration for Glare.

Eight MOHTB specimens were constructed from a single plate of Glare 2A-11/10-0.4. The code 2A indicates two layers of glass fibres oriented in the aluminum rolling direction for each prepreg ply. The ratio 11/10 refers to the number of aluminum and prepreg plies respectively. The last number refers to the thickness of each of the aluminum plies in the laminate (0.4 mm). The milled-out test section resulted in five Glare 2A-5/4-0.4 and three Glare 2A-6/5-0.4 specimens. Two 6/5 specimens were 100 mm wide, the remaining specimens were 50 mm wide. Table 1 describes the lay-up configurations for the test sections. Three Glare 2A-5/4-0.4 specimens were tested at 80 MPa to differing surface crack lengths. The remaining specimens were tested at 100 MPa. The tests were conducted on a 100 kN MTS fatigue test machine running TestStar software. All experiments were run at room temperature and normal lab air at a frequency of 10 Hz and a 0.1 stress ratio.

Table 1: Glare stack up sequences.

Layer	Constituent	
	Glare 2A-5/4-0.4	Glare 2A-6/5-0.4
1	0.4 mm Al2024-T3 L-T	0.4 mm Al2024-T3 L-T
2	0.256 mm 0°/0° Glass Fibre Prepreg	0. 256 mm 0°/0° Glass Fibre Prepreg
3	0.4 mm Al2024-T3 L-T	0.4 mm Al2024-T3 L-T
4	0. 256 mm 0°/0° Glass Fibre Prepreg	0. 256 mm 0°/0° Glass Fibre Prepreg
5	0.4 mm Al2024-T3 L-T	0.4 mm Al2024-T3 L-T
6	0. 256 mm 0°/0° Glass Fibre Prepreg	0. 256 mm 0°/0° Glass Fibre Prepreg
7	0.4 mm Al2024-T3 L-T	0.4 mm Al2024-T3 L-T
8	0. 256 mm 0°/0° Glass Fibre Prepreg	0. 256 mm 0°/0° Glass Fibre Prepreg
9	0.4 mm Al2024-T3 L-T	0.4 mm Al2024-T3 L-T
10		0. 256 mm 0°/0° Glass Fibre Prepreg
11		0.4 mm Al2024-T3 L-T

To obtain significant but reasonable bending in the specimens, a bending factor of at least 2.0 is desired. The Neutral Line Model generated the correct dimensions of the tapers in the specimens to achieve this goal. Specific samples were instrumented with strain gages to determine the actual bending factor and stress levels. Final values for k_b were:

k_b =2.2 for G2A-5/4-0.4 specimens tested at σ_{app} =80MPa

k_b =2.5 for G2A-5/4-0.4 specimens tested at σ_{app} =100MPa

k_b =2.0 for G2A-6/5-0.4 specimens tested at σ_{app} =100MPa

At regular fatigue cycle intervals, surface crack lengths were measured using a digital microscope. An optical endoscope was used to peer inside the open hole following each block of fatigue cycles to determine if a fatigue crack had initiated in a subsurface aluminium ply. Fatigue cracks were visible in the subsurface aluminum layers, as shown in Figure 6.

Each specimen was fatigued until a preset surface crack length was achieved. Following the fatigue tests, the sample was destructively inspected. The specimens were failed statically to expose the fatigue crack surfaces of all plies. The specimens were then placed in an oven at 350 degrees Celsius for four hours to burn away the adhesive in the prepreg between the aluminium plies. This exposed each of the aluminium plies enabling the determination of the final fatigue crack lengths in the subsurface plies. Results of the fatigue tests are given in the results section.
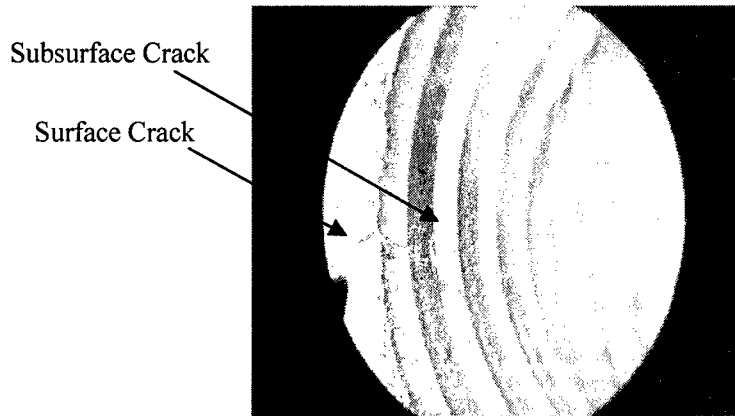
Figure 6: Typical endoscope view of subsurface crack initiation.

4. Results & Discussion

The key results of all experiments are listed in Table 2. For each condition the data for the left- and right-hand crack emerging from the open hole are listed. The data generated by this investigation are discussed in two sections: those pertaining to surface cracks and those pertaining to subsurface cracks. Surface crack data developed experimentally are presented as full crack growth curves which are compared to model predictions. For subsurface cracks, experiments necessarily provide only two data points per subsurface ply -- the cycles to crack initiation and final crack length at the end of the test. With the model presented above, the final subsurface crack length can be predicted once the cycles to crack initiation is known.

Table 2: Experimental Results

		Surface Crack		1st Subsurface Crack		2nd Subsurface Crack	
Sample Code	S_{app} (MPa)	N_{init} (kcycles)	a_{final} (mm)	N_{init} (kcycles)	a_{final} (mm)	N_{init} (kcycles)	a_{final} (mm)
MOHTB-1	80	66 /66	16.3 / 15.4	108 / 150	6.2 / 5.7	258 / 300	3.0 / 2.3
MOHTB-2	80	40 / 40	9.7 / 10.7	100 / 70	3.7 / 3.5	150 / 130	1.6 / 1.4
MOHTB-3	80	35 / 30	12.6 / 13.2	110 / 140	4.3 / 3.1		
MOHTB-4	100	35 / 25	17.4 / 18.6	40 / 55	5.5 / 3.8	100 / 80	2.3 / 2.5
MOHTB-5	100	25 / 25	17.6 / 16.9	45 / 55	5.7 / 4.0	80 / 95	3.3 / 2.8
MOHTB-6	100	40 / 50	9.1 / 9.4	45 / 50	6.9 / 6.5	80 / 50	3.9 / 5.0
MOHTB-7	100	50 / 70	39.4 / 40.2	70 / 60	28.8 / 30.1	80 / 60	21.6 / 21.6
MOHTB-8	100	40 / 40	25.3 / 33.0	60 / 60	21.8 / 24.9	70 / 70	15.0 / 17.7

Composite surface crack growth curves for all MOHTB specimens are shown in Figure 7. The data sets show crack propagation only; cycles for crack initiation have been left off. Superimposed on the curves are the analytical predictions of the model. The experimental data show good repeatability, with the usual expected scatter. Given the small number of samples tested, and the scatter inherent with fatigue testing, this data set appears legitimate.

For the extent of the testing conducted, the model matched the experimental data very well. Both the large differences in initial crack growth rate for different stress levels and different sample geometries and the differences in crack curves are well predicted by the model.

In the figure the initiation of subsurface cracks are indicated for sample G2A-6/5-0.4. Surprisingly, the occurrence of subsurface cracking did not affect the crack growth rate of the surface crack significantly. Similar results are obtained for the other two conditions.

For the model described here, no finite width correction was included for the crack opening stress intensities. This simplification appears justified, as the crack growth curves show no appreciable crack acceleration as the cracks grow. This is characteristic of Glare – the fibre bridging tends to slow down and regulate the crack growth in the material. Finite width effects tend not to be significant until much later in a part's life than that of a part made of monolithic aluminum.
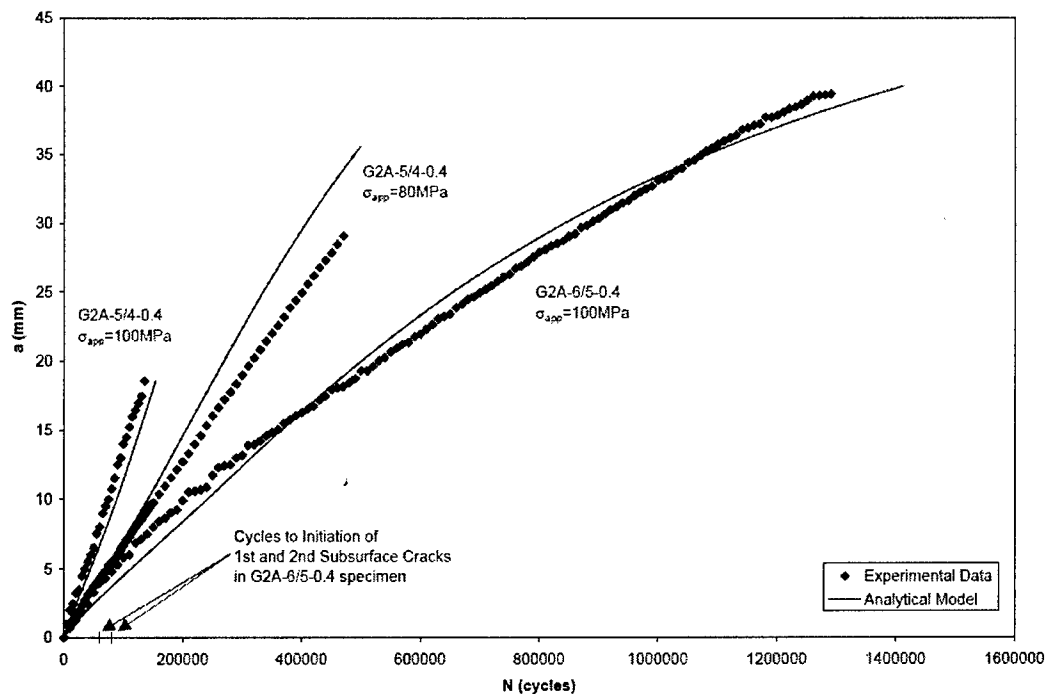

Figure 7: Surface crack propagation data. Cycles to initiation omitted.

Subsurface crack growth rates for all specimens are compared to the analytical model in Figures 8 a-c.

For the extent of the testing conducted, the model tracked well with the experimental data. The predictive accuracy drops significantly for deeper subsurface cracks. As the finite element data is limited to shorter subsurface cracks, a more refined fibre bridging stress distribution may be needed to accurately capture the crack growth character. The model over predicts the crack growth typically, so the model is conservative. For cracks beyond the length of those tested, it appears the model will under predict the crack growth.
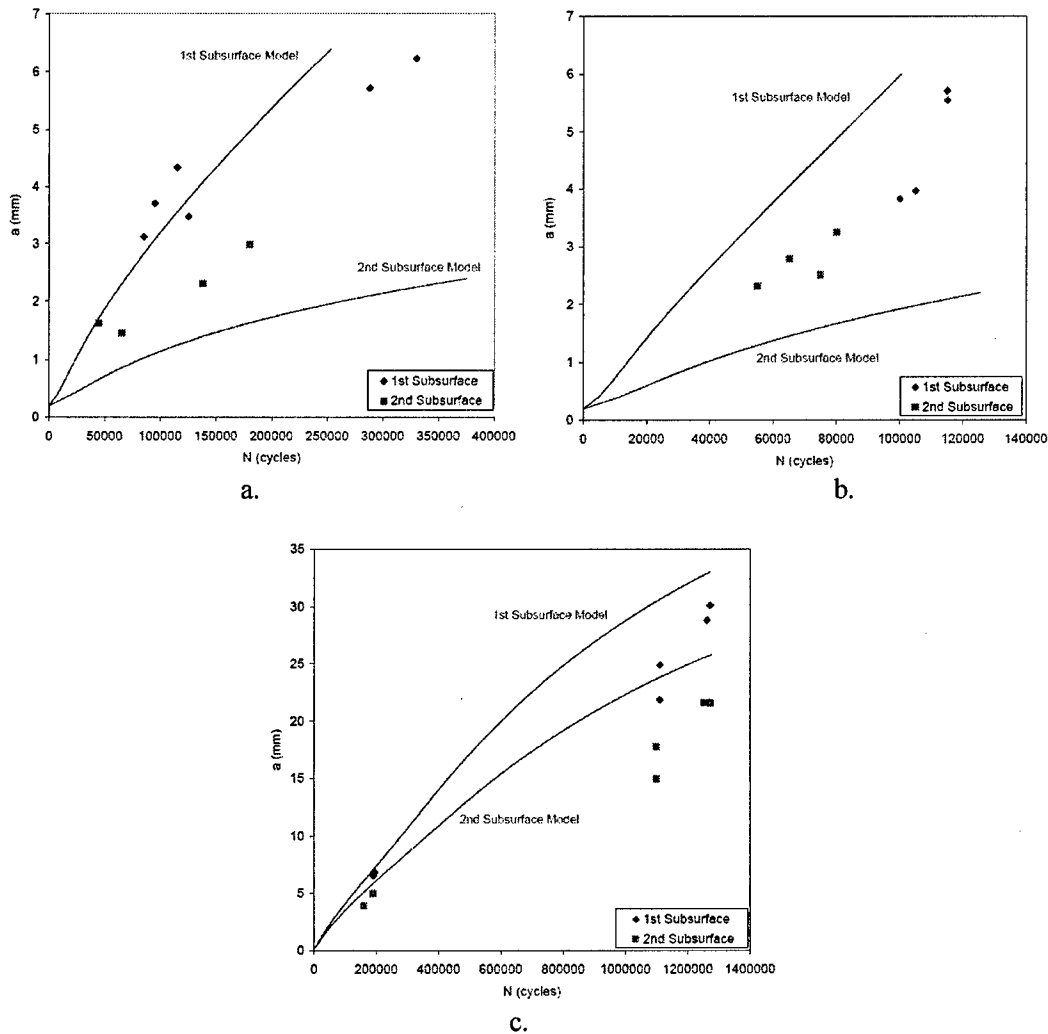
Figure 8: Subsurface crack propagation. a: G2A-5/4-0.4, Sapp=80MPa.
b. G2A-5/4-0.4, Sapp=100MPa. c. G2A-6/5-0.4, Sapp=100MPa.

5. Conclusions

An analytical/numerical crack growth model is developed to predict fatigue crack growth in the FML Glare subjected to combined tension and bending. The method is based on extracting fibre bridging stress predictions from finite element models and incorporating them into an analytical crack growth model.

The model was compared to experimental data for surface and subsurface cracks in Glare 2A specimens of varying thicknesses and applied stress levels. The results of the comparisons show that for surface cracks, the model accurately predicts the actual crack growth behavior of Glare 2A. For subsurface cracks, the method agreed well with experimental data.

6. Sources

[1] Marrissen R. Fatigue Crack Growth in ARALL. Delft University Press 1988, LR-574.

[2] Koning AU. Fatigue Crack Growth of Part Through the Thickness Cracks in Glare 3 and Glare 4B Coupons. National Aerospace Laboratory 2000, NLR CR 2000-078.

[3] Guo YJ, Wu XR, A Theoretical Model for Predicting Fatigue Growth Rates in Fiber Reinforced Metal Laminates. Fatigue Fract Engng Mater Struct 1998, 21:1133-45.

[4] Rose LRF. Theoretical Analysis of Crack Patching. Bonded Repair of Aircraft Structures, Dordrecht: Martinus Nijhoff Publishers, 1988, p.77-106.

[5] Fawaz S. A.. Fatigue Crack Growth in Riveted Joints. Delft University Press, 1997.

[6] Mortier W, Homan JJ. Crack Propagation in Surface Cracks and Part-Through Cracks. TU Delft 2002. B2V-02-31.

[7] Schijve J. Some Elementary Calculations on Secondary Bending in Simple Lap Joints. National Aerospace Laboratory 1972, NLR TR 72036 U.

[8] Tada H, Paris PC, Irwin GR. The Stress Analysis of Cracks Handbook. 2nd ed. St Louis (MO): Del Research Corporation, 1985.

[9] Alderliesten R. Fatigue Crack Propagation and Delamination Growth in Glare, Delft University Press 2005.

[10] Vlot A., Gunnink J. Fiber Metal Laminates an Introduction, Kluwer Academic Publishers, 2001

[11] Randell C, Zwaag S. On Subsurface Crack Growth in Fibre Metal Laminate Materials. International SAMPE Technical Conference, Dayton OH, 2003.

[12] Randell C. Development of the Milled Open Hole Tension Bending Specimen. International Journal of Fatigue, 2005